Fast Growth of Strain-Free AlN on Graphene-Buffered Sapphire

Yue Qi,[†,‡,§] Yunyu Wang,[∥,⊥] Zhenqian Pang,[#,∇] Zhipeng Dou,[†,○,◆] Tongbo Wei,*[,∥,⊥] Peng Gao,*[,†,○,◆,¶] Shishu Zhang,[†,‡] Xiaozhi Xu,[†,§,+] Zhenghua Chang,[#,∇] Bing Deng,[†,‡] Shulin Chen,[†,○,◆] Zhaolong Chen,[†,‡] Haina Ci,[†,‡,§] Ruoyu Wang,[†,‡] Fuzhen Zhao,[●] Jianchang Yan,[∥,⊥] Xiaoyan Yi,[∥,⊥] Kaihui Liu,[†,¶,+] Hailin Peng,[†,‡,◇] Zhiqiang Liu,[∥,⊥] Lianming Tong,[†,‡] Jin Zhang,[†,‡,◇] Yujie Wei,*[,#,∇] Jinmin Li,*[,∥,⊥] and Zhongfan Liu*[,†,‡,§,◇]
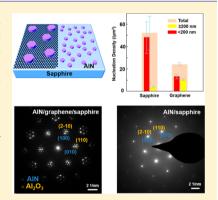
[†]Center for Nanochemistry (CNC), College of Chemistry and Molecular Engineering, [‡]Beijing National Laboratory for Molecular Sciences, [§]Academy for Advanced Interdisciplinary Studies, [○]Electron Microscopy Laboratory, School of Physics, [◆]International Center for Quantum Materials, and [+]State Key Laboratory for Mesoscopic Physics, School of Physics, Peking University, Beijing 100871, China

[∥]Research and Development Center for Solid State Lighting, Institute of Semiconductors, Chinese Academy of Sciences, Beijing 100083, China

[⊥]University of Chinese Academy of Sciences, Beijing 100049, China

[#]LNM, Institute of Mechanics, Chinese Academy of Sciences, Beijing, 100190, China

[∇]School of Engineering Sciences, University of Chinese Academy of Sciences, Beijing 100049, China

[¶]Collaborative Innovation Centre of Quantum Matter, Beijing 100871, China

[●]College of Science, China University of Petroleum, Qingdao 266580, China

[◇]Beijing Graphene Institute (BGI), Beijing 100095, China

S *Supporting Information*

ABSTRACT: We study the roles of graphene acting as a buffer layer for growth of an AlN film on a sapphire substrate. Graphene can reduce the density of AlN nuclei but increase the growth rate for an individual nucleus at the initial growth stage. This can lead to the reduction of threading dislocations evolved at the coalescence boundaries. The graphene interlayer also weakens the interaction between AlN and sapphire and accommodates their large mismatch in the lattice and thermal expansion coefficients; thus, the compressive strain in AlN and the tensile strain in sapphire are largely relaxed. The effective relaxation of strain further leads to a low density of defects in the AlN films. These findings reveal the roles of graphene in III-nitride growth and offer valuable insights into the efficient applications of graphene in the light-emitting diode industry.

INTRODUCTION

Epitaxial growth of group III-nitride films enables many optoelectronic devices such as light-emitting diodes (LEDs),[1,2] laser diodes (LDs),[3] ultraviolet (UV) emitters,[4] and high-frequency power electronics.[5,6] With the lack of native substrates (i.e., GaN and AlN) at economical cost, III-nitride films are always grown heteroepitaxially on various foreign substrates, for example, sapphire, silicon, and silicon carbide,[7−9] by using the metalorganic chemical vapor deposition (MOCVD) method. Such a growth route always produces severely stressed films with high-density defects (e.g., dislocations or stacking faults) due to the large mismatch in the lattice and thermal expansion coefficients between the substrate and epilayers.[10−12] These defects could detrimentally degrade the device performance (e.g., efficiency, reliability, and life) by acting as nonradiative recombination sites or a leakage

current pathway.[13,14] In order to achieve high-quality III-nitride films,[15−17] buffer layers of low-temperature grown AlN or GaN are generally required to minimize the mismatch effect.

Notably, in addition to the defects introduced by the lattice and thermal mismatches between the substrate and epilayers, a high density of threading dislocations (TDs) also evolves during the coalescence of separated three-dimensional (3-D) islands of III-nitrides. This type of TD is always vertical to the substrate and can propagate through the thickness into the quantum well layers. It is even worse that these TDs have no possibility to react with each other to be eliminated during the subsequent thickness increase.[18] However, reducing the density of the islands and simultaneously increasing the
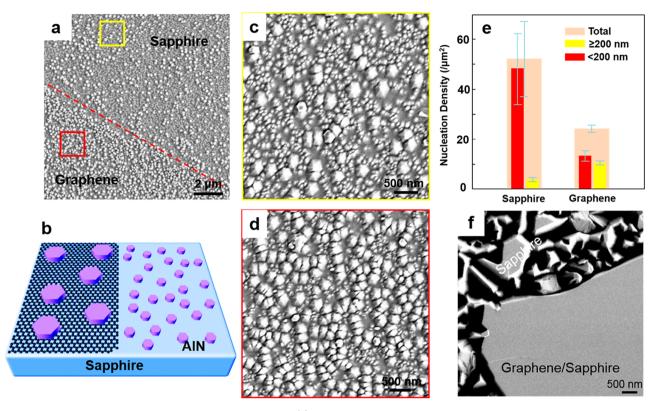
Figure 1. Effects of the graphene interlayer on the AlN nucleation. (a) Large-scale SEM image showing the nucleation of AlN on bare sapphire and graphene-buffered sapphire (growth duration: ∼ 6 min). (b) Corresponding schematic. (c, d) Magnified SEM images showing the distributions of the AlN nucleus on bare sapphire (c) and graphene-buffered sapphire (d). (e) Statistics of the density and size of the AlN nucleus on sapphire and graphene/sapphire. (f) SEM image for the noncoalesced and coalesced AlN domains on sapphire and graphene/sapphire, respectively.

domain size at the nucleation stage are effective to reduce the density of TDs.[19,20]

In order to improve the quality of III-nitride films, many materials have been proposed to act as the buffer layers including graphene. As one of the typical two-dimensional (2-D) materials, graphene has no dangling bond on the surface but possesses a hexagonal arrangement of atoms similar to the (0001) *c* plane of III-nitrides (e.g., AlN). Maturely, large-scale single-crystal graphene could be synthesized with the chemical vapor deposition (CVD) method.[21−23] By using graphene as the buffer layer, the effects of the lattice mismatch between AlN (or GaN) and graphene (∼26.4% or ∼29.6%)[24−26] are no longer significant due to the quasi-van der Waals epitaxy growth for III-nitrides on graphene. Additionally, the inert surface of graphene could weaken the nucleation of III-nitrides, and the low migration barrier of metals on graphene allows the adatoms to diffuse easily, which promotes the 2-D lateral growth of nitride islands and thus reduces the density of TDs formed at the coalesced boundaries.[26−28] Consequently, the quality of III-nitrides synthesized through the graphene-buffered route could be comparable to that of the conventional AlN- (GaN)-buffered route.[29] Moreover, benefiting from the weak interactions between graphene interlayers and graphene epilayers, the upper LEDs could be easily transferable onto foreign substrates such as metal or plastic, to improve the thermal conductivity of the device or to achieve the ideal flexibility.[29,30] Nevertheless, in the graphene-buffered growth route, the roles of graphene are still ambiguous, including the effects of graphene on the growth rate and stain relaxation of nitride films. These issues are imperative for the effective applications of graphene in the LED industry.

In this work, graphene is used as the buffer layer for AlN growth on sapphire (α-Al$_2$O$_3$(0001)), and it brings two important advantages. First, with the presence of graphene, the nucleation density of AlN is decreased, and the growth rate of the individual nucleus is increased. As a result, the density of TDs evolved at the coalescence boundaries is significantly reduced. Second, the strains in both AlN and sapphire are largely reduced by the introduction of graphene, which could further lower the density of misfit dislocations in the epilayers, and the enhancement of the efficiency of the LEDs is expected. These findings shed light on the growth of high-quality semiconducting nitride films via graphene engineering.

■ RESULTS AND DISCUSSION

Single-crystal monolayer graphene grown on Cu(111) foils was transferred onto a sapphire substrate, with the surface being kept flat and clean (scanning electron microscopy (SEM) images in Figure S1). The Raman spectrum of graphene transferred onto sapphire in Figure S1e showed a low or even negligible D peak and an intense, narrow 2D peak, which implied the high quality of the graphene.[31] Subsequently, the MOCVD method was used for AlN growth on the obtained graphene/sapphire substrate. At the initial stage of growth, the graphene covering on the surface imposes obvious effects on the nucleation density of AlN and the growth rate of the individual nucleus. The SEM image in Figure 1a presents the AlN nucleation on bare (upper right) and graphene-covered sapphire (bottom left). The two typical regions can be easily distinguished from the different nucleation density and domain size of AlN, as schematically shown in Figure 1b. The statistics from the magnified SEM images in Figure 1c, d show that the
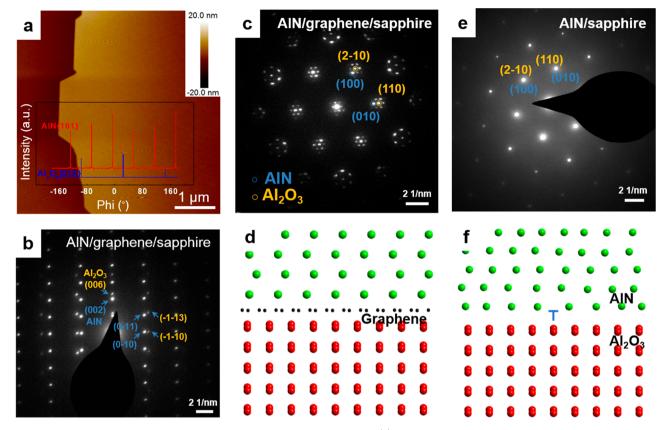
Figure 2. Effects of the graphene buffer layer on the strains in AlN and sapphire. (a) AFM image for the AlN films grown on graphene/sapphire. Inset: XRD phi scan of AlN/graphene/sapphire, showing the good large-scale epitaxial relationship between AlN and sapphire. (b) SAED pattern from the interface region of the AlN/graphene/sapphire cross-sectional sample. (c, e) SAED patterns of the AlN/graphene/sapphire (c) and the AlN/sapphire (e) planar view samples. (d, f) Schematics for the two types of interfaces. Only Al and C atoms are visible for clarity. In (b), the zone axes of sapphire and AlN are $[1-10]$ and $[100]$, respectively. In (c, e), the axis is along $[001]$.

nucleus densities of AlN are 41 μm^{-2} on sapphire and 23 μm^{-2} on graphene/sapphire (Figure 1e). This result implies that graphene can suppress the AlN nucleation, which is likely attributed to the lack of dangling bonds on the surface. Furthermore, the densities of the AlN domain with a diagonal distance larger than 200 nm on sapphire and graphene/sapphire are 3 and 11 μm^{-2}, respectively. These different growth rates of AlN on the two types of regions are possibly due to the fact that graphene could reduce the diffusion barrier of metals and make adatoms diffuse easily with large diffusion lengths, which accelerates the 2-D lateral growth of the islands on graphene-covered sapphire with respect to that on bare sapphire. Moreover, the same tendency was also observed when the nucleation time was reduced to ~3 min (Figure S2). Notably, the orientations of the separated AlN islands on graphene/sapphire are well aligned, as evidenced by the selected area electron diffraction pattern (SAED) in Figure S3. In addition, the AlN nucleation density could increase at the domain edges and wrinkles of graphene due to the rich dangling bonds at the domain edges and the enhanced chemical reactivity at the wrinkles, which is caused by the increased strain energy induced by the local mechanical deformation of graphene.

During the subsequent coalescence of these separated 3-D islands, TDs vertical to the substrate always evolved at the coalescence boundaries. These types of TDs have no possibility to react with each other and thus cannot be eliminated by increasing the thickness.[18,32−34] In this regard,

on graphene/sapphire, the lower nucleation density and larger domain size of the AlN nucleus can effectively reduce the formation of TDs. When the growth duration is extended to ~60 min, AlN coalesces to form flat films on graphene/sapphire, which is in sharp contrast to the noncoalesced, rough islands on the bare sapphire counterpart (SEM images in Figure 1f and Figure S1f). Notably, the Raman spectra in Figures S4a, b and S5a, b prove the existence of graphene in the coalesced regions while the absence in the noncoalesced AlN regions, respectively. The cathodoluminescence (CL) spectrum from AlN/graphene/sapphire shows a narrower full width at half-maximum (fwhm) and a stronger intensity than those from AlN/sapphire (peaks at ~210.6 nm for AlN), indicating the higher quality of the films (Figure S6). The characterization of the X-ray diffraction (XRD) rocking curve shows that, with the introduction of graphene, the density of the screw dislocation decreased from 8.01×10^{8} to 2.81×10^{8} cm^{-2} and the density of the edge dislocation decreased from 5.88×10^{9} to 4.63×10^{9} cm^{-2}. Notably, the new growth process of the AlN films with the introduction of the graphene interlayer bypasses the native buffer layers growth commonly used in the traditional two-step MOCVD method.

For AlN directly grown on sapphire, because of the large mismatch in the lattice and thermal expansion coefficients, severe strains always remain in the film and substrate (lattice constants: a_{AlN} = 0.3112 nm, $a_{sapphire}$ = 0.4758 nm; mean expansion coefficients along the a axes: α_{AlN} = 5.3×10^{-6} $°C^{-1}$, $\alpha_{sapphire}$ = 7.3×10^{-6} $°C^{-1}$).[35] The graphene buffer layer can
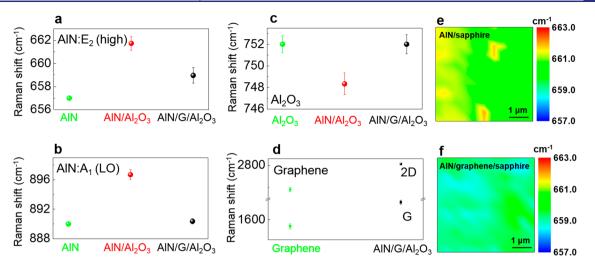
Figure 3. Strains in AlN/sapphire and AlN/graphene/sapphire characterized by Raman spectroscopy. (a, b) Relative Raman shifts of the E_2 (high) (a) and A_1 (LO) peaks (b) of AlN in pristine AlN, AlN/sapphire, and AlN/graphene/sapphire, respectively. (c) Relative Raman shifts of sapphire in pristine sapphire, AlN/sapphire, and AlN/graphene/sapphire. (d) Relative Raman shifts of G and 2D peaks of graphene in pristine graphene and AlN/graphene/sapphire. (e, f) Raman mappings (5 μm × 5 μm) of the E_2 (high) peak of AlN in AlN/sapphire and AlN/graphene/sapphire, respectively.

help release the strains in the film and substrate. The surface of the as-grown AlN film on graphene/sapphire is flat, presenting an atomic terrace in the atomic force microscopy (AFM) image in Figure 2a. The XRD in Figure S7a and the cross-sectional SAED in Figure 2b confirm the epitaxial relationship between AlN and sapphire and indicate that the growth direction (out-of-plane orientation) is (0002). In addition, the large-scale epitaxial growth of AlN on the graphene-covered sapphire is investigated by XRD phi scan (inset in Figure 2a) and low-energy electron diffraction (LEED) characterizations (Figure S7b). In Figure 2b, there are two separate sets of diffraction reflections along the growth direction [001] and in the a/b planes, indicating that sapphire and AlN maintain their respective lattice structures and the strain between them has been largely relaxed due to the presence of graphene. The SAED patterns along the [001] direction of the AlN/graphene/sapphire and AlN/sapphire plane samples are presented in Figure 2c, e, respectively. The relaxed structure in AlN/graphene/sapphire is further confirmed by the satellite spot diffraction patterns of the planar view specimen in Figure 2c. The satellite spots are caused by double diffraction; that is, the beams are first diffracted by AlN and subsequently diffracted by sapphire (or vice versa). The satellite spot diffraction patterns confirm that sapphire and AlN maintain their respective lattice structures, which also indicates the strains in AlN and sapphire are relaxed, as schematically shown in Figure 2d. In comparison, a single set of diffraction patterns is observed for AlN on bare sapphire in Figure 2e for the reason that the lattice of AlN is fully clamped and aligned with the sapphire substrate. When AlN is epitaxially grown on the bare sapphire substrate, the in-plane lattice of AlN is fully constrained by the sapphire substrate. Their reflections in the SAED patterns are therefore overlapped with each other, showing a single setlike pattern in Figure 2e. In this case, significant strain should exist in AlN, as shown in Figure 2f. The element mappings in Figure S8 implied the existence of sapphrie under AlN in the sample in Figure 2e. In addition, these SAED patterns in Figure 2c, e also indicated that the graphene buffer layer did not change the orientation of AlN on sapphire. The cross-sectional SAEDs of the single AlN and

graphene/sapphire materials are presented in Figure S9 for reference.

The strains in AlN and sapphire could impose profound effects on their Raman spectra; for example, the E_2 (high) mode of AlN around 655 cm^{-1} could provide a clear signature for the biaxial strain within the basal plane.[36−38] The full spectra from the samples of bare sapphire, AlN/sapphire, and AlN/graphene/sapphire are shown in Figure S10. For reference sapphire, there are three typical peaks at ∼419.2, ∼580.1, and ∼751.2 cm^{-1} (Figure S10a), and for the reference AlN, the representative peaks are located around 248.0 (E_2 (low)), 657.0 (E_2 (high)), and 890.0 cm^{-1} (A_1 (LO)) (Figure S10b, c).[39,40] Specifically, from Figure 3a and Figure S10d, the strain-sensitive E_2 (high) peaks from AlN/graphene/sapphire were located at a lower wavenumber of ∼658.9 cm^{-1}, much closer to the pristine one (∼657.0 cm^{-1}) as compared to that of AlN/sapphire (∼661.7 cm^{-1}), which suggests the compressive strain in AlN is significantly relaxed. The same conclusion can be obtained from the analysis of A_1 (LO) peaks (∼890.4 cm^{-1} for AlN/graphene/sapphire, ∼890.0 cm^{-1} for bulk AlN, and ∼896.7 cm^{-1} for AlN/sapphire (Figure 3b and Figure S10e)). For sapphire in Figure 3c, the strain-sensitive peak from AlN/graphene/sapphire is ∼752.0 cm^{-1} (black), much closer to the reference one (green), while it shifts to the much lower wavenumber of ∼748.3 cm^{-1} (red) for AlN/sapphire, further confirming that the tensile strain in sapphire of AlN/graphene/sapphire is also reduced. Figure 3e, f is the Raman mappings (5 μm × 5 μm) of the E_2 (high) peak of AlN in AlN/sapphire and AlN/graphene/sapphire, respectively, which showed that, at a large scale, the E_2 (high) peak of AlN in AlN/sapphire shifted to a much higher wavenumber and the peak in AlN/graphene/sapphire was much closer to the pristine one. In addition, the analysis about the changes of the lattice parameters of AlN based on the XRD measurements is also presented in Table 1 in the Supporting Information to illustrate the strain differences in the systems of AlN/graphene/sapphire, AlN/graphene, and bulk AlN.

Notably, the 2D and G peaks of graphene also exhibit high stain sensitivity. A previous study reported that, under the uniaxial tensile strain, the 2D and G peaks of monolayer
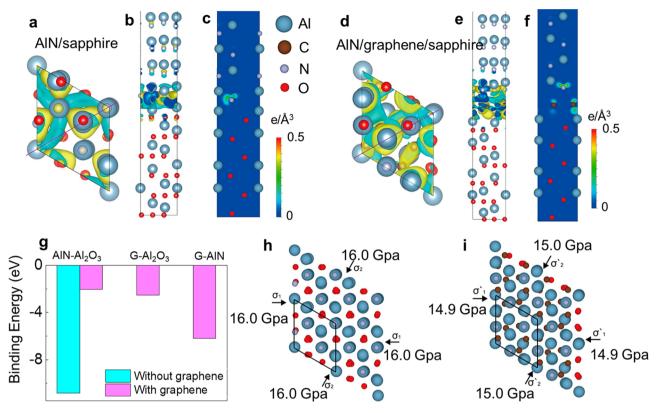
Figure 4. DFT calculations of the AlN/Al$_2$O$_3$ BE and the internal stress in AlN. (a, d) Calculated models of AlN/sapphire and AlN/graphene/sapphire, respectively. The black parallelogram denotes the calculation cell. (b, e) Front view of the 3-D charge density corresponding to (a, d), respectively. The yellow and blue regions represent the electron gain and loss, respectively. (c, f) Sections of charge density along the purple line in (a, b), respectively. (Units of the contours: e Å^{-3}). (g) Calculated BEs for AlN/Al$_2$O$_3$ in AlN/sapphire and AlN/graphene/sapphire are −10.84 and −2.04 eV, respectively, and −6.20 eV for G-AlN and −2.51 eV for G-Al$_2$O$_3$. (h, i) Calculated internal stress in AlN without (g) and with (h) the graphene interlayer (16.0 and 14.9 GPa, respectively).

graphene present significant red shifts with 27.8 and 14.2 cm^{-1} per 1%, respectively.[41] Under the biaxial strain introduced by graphene bubbles, the G peak could decrease from 1598 to 1525 cm^{-1}, and the 2D peak could move from 2695 to 2552 cm^{-1}.[42] In the current work, when graphene is sandwiched between AlN and sapphire, its G and 2D peaks shifted to the much higher wavenumbers of ∼1648.3 and ∼2810.3 cm^{-1}, respectively, with regard to those of the pristine ones (∼1581.6 and ∼2676.9 cm^{-1}, respectively) (Figure 3d). Because of the negative expansion coefficient of graphene (approximately −7 × 10^{-6} K^{-1}) and the positive expansion coefficients of AlN and sapphire (α_{AlN} = 5.3 × 10^{-6} °C^{-1}, $\alpha_{sapphire}$ = 7.3 × 10^{-6} °C^{-1}),[35] the strong compressive strain imposes graphene during cooling after the MOCVD growth, which mainly accounts for such a large shift. The values of the peak positions in Figure 3 are detailed in Figure S11.

To better understand the roles of graphene in the strain relaxation during the AlN growth on sapphire, density functional theory (DFT) calculations are performed to extract the AlN/sapphire (AlN/Al$_2$O$_3$) binding energy (BE) and the internal stress in the AlN film. Figure 4a, d shows the calculated models of AlN/sapphire and AlN/graphene/sapphire, respectively. In the front view of the 3-D charge density in Figure 4b, e, obvious charge redistribution can be observed after graphene insertion. In AlN/sapphire, there exists prominent charge exchange between the N in AlN and the Al in Al$_2$O$_3$ (Figure 4b, c). After graphene insertion, the charge exchange happens among all the interfaces of graphene (G)-AlN and G-Al$_2$O$_3$ (Figure 4e, f), and the resulting strong

interactions (−2.51 eV for G-Al$_2$O$_3$ and −6.20 eV for G-AlN, Figure 4g) lead to the distortion of the graphene layer (Figure S12), which can explain the strong compressive strain introduced in graphene. The calculated AlN/Al$_2$O$_3$ BEs are −10.84 eV for AlN/sapphire and −2.04 eV for AlN/graphene/sapphire (Figure 4g). The weakened AlN/Al$_2$O$_3$ interaction in AlN/graphene/sapphire largely accommodates their lattice and thermal mismatches; thus, the compressive strain in AlN is largely released. The calculated internal stress in AlN is reduced from 16.0 GPa in AlN/sapphire to 14.9 GPa in AlN/graphene/sapphire (Figure 4h, i), which is in excellent agreement with electron microscopy and Raman characterizations.

■ SUMMARY

In summary, the introduction of the graphene buffer layer between AlN and sapphire can reduce the nucleation density and increase the growth rate of the AlN nuclei. As a result, the TDs evolved at the coalescence boundaries are obviously decreased; thus, the film quality is increased. Simultaneously, the graphene buffer layer significantly weakens the AlN/Al$_2$O$_3$ interaction, which accommodates their large lattice and thermal mismatches. Thus, the compressive strain in AlN and the tensile strain in sapphire are largely relaxed. High energy efficiency of the LEDs that are fabricated from the strain-free AlN film can be expected. This work reveals the role of the graphene buffer layer in the growth of III-nitrides, which provides instructions for the use of graphene in the LED industry.

EXPERIMENTAL SECTION

Graphene Synthesis. Graphene was grown on Cu(111) foils through the CVD method at ~1000 °C with 10 sccm CH_4 (0.1% diluted in Ar) being introduced into the system.

AlN Growth. The AlN film was grown with a low-pressure MOCVD (~50 Torr) method, using trimethylaluminum (50 sccm) and NH_3 (500 sccm) as the Al and N precursors and H_2 (12 SLM) as the carrier gas. It is a one-step process here without using LT-buffer layers, and the HT-AlN was grown at a nominal temperature of 1200 °C for 1 h.

Graphene Transferring Process. Poly(methyl methacrylate) (PMMA, 4 wt %) was first spin-coated on the graphene/Cu substrates at the speed of 2000 rpm for 1 min and cured at 170 °C for 3 min. Then, Cu was etched using 1 M $Na_2S_2O_8$ (aq) as etchant for about 1 h. After etching, the PMMA/graphene film was merged into DI water to clean the residues. The PMMA/graphene was then rinsed in DI water several times and attached to the sapphire substrates. After drying in air through baking at 170 °C for 5 min, the PMMA was removed by hot acetone.

Characterization. The prepared samples were characterized using SEM (Hitachi S-4800, operating at 1 kV) and Raman spectroscopy (WITec alpha300 RS). The cross-transmission electron microscopy (TEM) sample was fabricated using a focused ion beam system (FIB, FET Strata DB 235). The TEM and SAED were performed on a Tecnai F20 at 200 kV, and the scanning TEM was acquired using a FEI cubed double corrected Themis G2300 operated at 300 kV. AFM morphology imaging was carried out on a Bruker Dimension Icon. The XRD was measured with a Rigaku (D/MAX 2500PC).

ASSOCIATED CONTENT

⑤ Supporting Information

The Supporting Information is available free of charge on the ACS Publications website at DOI: 10.1021/jacs.8b03871.

> SEM images; Raman spectra and peak positions; SAED patterns; CL spectra; XRD and LEED characterizations; analysis of lattice parameters; element mapping; TEM images; and DFT calculations (PDF)

AUTHOR INFORMATION

Corresponding Authors

*tbwei@semi.ac.cn
*p-gao@pku.edu.cn
*yujie_wei@lnm.imech.ac.cn
*jmli@semi.ac.cn
*zfliu@pku.edu.cn

ORCID ⓘ

Peng Gao: 0000-0003-0860-5525
Kaihui Liu: 0000-0002-8781-2495
Hailin Peng: 0000-0003-1569-0238
Lianming Tong: 0000-0001-7771-4077
Jin Zhang: 0000-0003-3731-8859
Yujie Wei: 0000-0002-3213-7891
Zhongfan Liu: 0000-0003-0065-7988

Notes

The authors declare no competing financial interest.

ACKNOWLEDGMENTS

REFERENCES

(1) Nakamura, S.; Mukai, T.; Senoh, M. *J. Appl. Phys.* **1994**, *76*, 8189−8191.

(2) Nakamura, S.; Krames, M. R. P. *Proc. IEEE* **2013**, *101*, 2211−2220.

(3) Nakamura, S.; Senoh, M.; Nagahama, S.; Iwasa, N.; Yamada, T.; Matsushita, T.; Kiyoku, H.; Sugimoto, Y. *Jpn. J. Appl. Phys.* **1996**, *35*, L74−L76.

(4) Kneissl, M.; Kolbe, T.; Chua, C.; Kueller, V.; Lobo, N.; Stellmach, J.; Knauer, A.; Rodriguez, H.; Einfeldt, S.; Yang, Z.; Johnson, N. M.; Weyers, M. *Semicond. Sci. Technol.* **2011**, *26*, 014036.

(5) Binari, S. C.; Redwing, J. M.; Kelner, G.; Kruppa, W. *Electron. Lett.* **1997**, *33*, 242−243.

(6) Mishra, U. K.; Parikh, P.; Wu, Y.-F. *Proc. IEEE* **2002**, *90*, 1022−1031.

(7) Hemmingsson, C.; Paskov, P. P.; Pozina, G.; Heuken, M.; Schineller, B.; Monemar, B. *J. Cryst. Growth* **2007**, *300*, 32−36.

(8) Zhang, J. X.; Qu, Y.; Chen, Y. Z.; Uddin, A.; Yuan, S. *J. Cryst. Growth* **2005**, *282*, 137−142.

(9) Ponce, F. A.; Krusor, B. S.; Major, J. S.; Plano, W. E.; Welch, D. F. *Appl. Phys. Lett.* **1995**, *67*, 410−412.

(10) Nakamura, S. *Science* **1998**, *281*, 956−961.

(11) Schubert, M. F.; Chhajed, S.; Kim, J. K.; Schubert, E. F.; Koleske, D. D.; Crawford, M. H.; Lee, S. R.; Fischer, A. J.; Thaler, G.; Banas, M. A. *Appl. Phys. Lett.* **2007**, *91*, 231114.

(12) Hemmingsson, C.; Pozina, G. *J. Cryst. Growth* **2013**, *366*, 61−66.

(13) Rosner, S. J.; Carr, E. C.; Ludowise, M. J.; Girolami, G.; Erikson, H. I. *Appl. Phys. Lett.* **1997**, *70*, 420−422.

(14) Sugahara, T.; Sato, H.; Hao, M. S.; Naoi, Y.; Kurai, S.; Tottori, S.; Yamashita, K.; Nishino, K.; Romano, L. T.; Sakai, S. *Jpn. J. Appl. Phys.* **1998**, *37*, L398−L400.

(15) Liu, L.; Edgar, J. H. *Mater. Sci. Eng., R* **2002**, *37*, 61−127.

(16) Meng, W. J.; Perry, T. A. *J. Appl. Phys.* **1994**, *76*, 7824−7828.

(17) Kim, C.; Robinson, I. K.; Myoung, J.; Shim, K. H.; Kim, K. *J. Appl. Phys.* **1999**, *85*, 4040−4044.

(18) Mathis, S. K.; Romanov, A. E.; Chen, L. F.; Beltz, G. E.; Pompe, W.; Speck, J. S. *J. Cryst. Growth* **2001**, *231*, 371−390.

(19) Haffouz, S.; Lahreche, H.; Vennegues, P.; de Mierry, P.; Beaumont, B.; Omnes, F.; Gibart, P. *Appl. Phys. Lett.* **1998**, *73*, 1278−1280.

(20) Datta, R.; Kappers, M. J.; Vickers, M. E.; Barnard, J. S.; Humphreys, C. *Superlattices Microstruct.* **2004**, *36*, 393−401.

(21) Deng, B.; Pang, Z.; Chen, S.; Li, X.; Meng, C.; Li, J.; Liu, M.; Wu, J.; Qi, Y.; Dang, W.; Yang, H.; Zhang, Y.; Zhang, J.; Kang, N.; Xu, H.; Fu, Q.; Qiu, X.; Gao, P.; Wei, Y.; Liu, Z.; Peng, H. *ACS Nano* **2017**, *11*, 12337−12345.

(22) Li, B. W.; Luo, D.; Zhu, L.; Zhang, X.; Jin, S.; Huang, M.; Ding, F.; Ruoff, R. S. *Adv. Mater.* **2018**, *30*, 1706504.

(23) Xu, X.; Zhang, Z.; Dong, J.; Yi, D.; Niu, J.; Wu, M.; Lin, L.; Yin, R.; Li, M.; Zhou, J.; Wang, S.; Sun, J.; Duan, X.; Gao, P.; Jiang, Y.; Wu, X.; Peng, H.; Ruoff, R. S.; Liu, Z.; Yu, D.; Wang, E.; Ding, F.; Liu, K. *Sci. Bull.* **2017**, *62*, 1074−1080.

(24) Leszczynski, M.; Teisseyre, H.; Suski, T.; Grzegory, I.; Bockowski, M.; Jun, J.; Porowski, S.; Pakula, K.; Baranowski, J. M.; Foxon, C. T.; Cheng, T. S. *Appl. Phys. Lett.* **1996**, *69*, 73−75.

(25) Tanaka, M.; Nakahata, S.; Sogabe, K.; Nakata, H.; Tobioka, M. *Jpn. J. Appl. Phys.* **1997**, *36*, L1062−L1064.

(26) Alaskar, Y.; Arafin, S.; Wickramaratne, D.; Zurbuchen, M. A.; He, L.; McKay, J.; Lin, Q.; Goorsky, M. S.; Lake, R. K.; Wang, K. L. *Adv. Funct. Mater.* **2014**, *24*, 6629−6638.

(27) Chan, K. T.; Neaton, J. B.; Cohen, M. L. *Phys. Rev. B: Condens. Matter Mater. Phys.* **2008**, *77*, 235430.

(28) Al Balushi, Z. Y.; Miyagi, T.; Lin, Y.-C.; Wang, K.; Calderin, L.; Bhimanapati, G.; Redwing, J. M.; Robinson, J. A. *Surf. Sci.* **2015**, *634*, 81−88.

(29) Kim, J.; Bayram, C.; Park, H.; Cheng, C.-W.; Dimitrakopoulos, C.; Ott, J. A.; Reuter, K. B.; Bedell, S. W.; Sadana, D. K. *Nat. Commun.* **2014**, *5*, 4836.

(30) Chung, K.; Lee, C.-H.; Yi, G.-C. *Science* **2010**, *330*, 655−657.

(31) Li, X. S.; Cai, W. W.; An, J.; Kim, S.; Nah, J.; Yang, D. X.; Piner, R.; Velamakanni, A.; Jung, I.; Tutuc, E.; Banerjee, S. K.; Colombo, L.; Ruoff, R. S. *Science* **2009**, *324*, 1312−1314.

(32) Wu, X. H.; Fini, P.; Tarsa, E. J.; Heying, B.; Keller, S.; Mishra, U. K.; DenBaars, S. P.; Speck, J. S. *J. Cryst. Growth* **1998**, *189-190*, 231−243.

(33) Lang, T.; Odnoblyudov, M. A.; Bougrov, V. E.; Romanov, A. E.; Suihkonen, S.; Sopanen, M.; Lipsanen, H. *Phys. Status Solidi A* **2006**, *203*, R76−R78.

(34) Sugawara, Y.; Ishikawa, Y.; Watanabe, A.; Miyoshi, M.; Egawa, T. *Jpn. J. Appl. Phys.* **2016**, *55*, 05FB08.

(35) Lee, J. E.; Ahn, G.; Shim, J.; Lee, Y. S.; Ryu, S. *Nat. Commun.* **2012**, *3*, 1024.

(36) Trodahl, H. J.; Martin, F.; Muralt, P.; Setter, N. *Appl. Phys. Lett.* **2006**, *89*, 061905.

(37) Prokofyeva, T.; Seon, M.; Vanbuskirk, J.; Holtz, M.; Nikishin, S. A.; Faleev, N. N.; Temkin, H.; Zollner, S. *Phys. Rev. B: Condens. Matter Mater. Phys.* **2001**, *63*, 125313.

(38) Sarua, A.; Kuball, M.; Van Nostrand, J. E. *Appl. Phys. Lett.* **2002**, *81*, 1426−1428.

(39) Kadleikova, M.; Breza, J.; Vesely, M. *Microelectron. J.* **2001**, *32*, 955−958.

(40) Davydov, V. Y.; Kitaev, Y. E.; Goncharuk, I. N.; Smirnov, A. N.; Graul, J.; Semchinova, O.; Uffmann, D.; Smirnov, M. B.; Mirgorodsky, A. P.; Evarestov, R. A. *Phys. Rev. B: Condens. Matter Mater. Phys.* **1998**, *58*, 12899−12907.

(41) Ni, Z. H.; Yu, T.; Lu, Y. H.; Wang, Y. Y.; Feng, Y. P.; Shen, Z. X. *ACS Nano* **2008**, *2*, 2301−2305.

(42) Zabel, J.; Nair, R. R.; Ott, A.; Georgiou, T.; Geim, A. K.; Novoselov, K. S.; Casiraghi, C. *Nano Lett.* **2012**, *12*, 617−621.